## 1 Title

# Shale Compaction Kinetics

## 2 Authors Information

By James Edward Smith*, Phillips Petroleum, ret., and
Edward Millard Smith-Rowland**, Alion Corp.
*Corresponding author; edsmith6@hotmail.com. 1209 Harris Dr, Bartlesville, OK 74006.
** 3dw4rd@verizon.net. 3113 Edgewood Rd, Ellicott City, MD 21043-3419.

## 3 Abstract

The grain-to-grain stress vertically in sediments is given by the overburden less the pore fluid pressure, $\sigma$, divided by the fraction of the horizontal area which is the supporting matrix , $(1-\varphi)$, $\varphi$ being the porosity. It is proposed that the fractional reduction of this ratio, $\Lambda$, with time is given by the product of $\varphi^{4m/3)}$, $(1-\varphi)^{4n/3}$, and one or more Arrhenius functions $a\exp(-E/RT)$ with m and n close to 1. This proposal is tested for shale sections in six wells from around the world for which porosity-depth data are available. Good agreement is obtained above 30-40 C. A single activation energy of 24+-6 kJ/mole, indicating pressure solution of quartz, 24 kJ/mol, was obtained. The average value of m is 1, indicating fractal pore-matrix spaces and water-wet interfaces. Grain-to -grain interfaces may be fractal with n close to 1, but can have lower values suggesting smooth surfaces in younger rocks. Results are independent of over- or under-pressure of pore water. This model explains shale compaction quantitatively. Given porosity-depth data and accurate activation energy, E, one can infer maximum paleo-geothermal-gradient and from that organic maturity, thus avoiding unnecessary drilling.

## 4 Keywords

Shale compaction, kinetics, activation energy, pore interfaces, grain interfaces, fractals, organic maturity

# 5 Introduction

For overburden $S$ and pore pressure $p$, the vertical stress difference

$$\sigma \equiv (S - p), \tag{1}$$

can be changed by sedimentation, erosion or fluid flow through rock in this one-dimensional model. Similarly $\sigma$ divided by the fractional area of solid matrix $(1-\varphi)$ supporting this stress can be relieved by pressure solution, breakage, relative movement of grains or fluid flow.

$$\Lambda \equiv (S - p)/(1 - \varphi) = \sigma/(1 - \varphi). \tag{2}$$

Differentiating with respect to time gives

$$\frac{dln\Lambda}{dt} = - \frac{dln(1-\varphi)}{dt} + \frac{dln\sigma}{dt} \, . \tag{3}$$

The first term deals with local porosity changes, while the second term deals with deposition, erosion, and fluid flow. The second term was treated previously(Smith 1971,1973; Smith, Dysinger and Borst 1980).
Focus here is on the first term, proposing and supporting with data a chemical-type expression describing the time evolution of the vertical grain-to-grain pressure, or frame pressure.

# 6 Kinetic Equation and Experimental Tests

It is proposed that the reactions to reduce the frame pressure are proportional to the frame pressure $\Lambda$, to the pore surface area, $\varphi^{1.33}$, to the frame surface area, $(1-\varphi)^{1.33}$, and to one (or a sum of) Arrhenius factors, $a \exp -E/RT$. The exponent $1.33 = 4/3$ is the fractal dimension of a percolation front and twice the surface dimension 2/3 of smooth solids. R is the ideal gas constant (8.314J/(mol degK), T is temperature in Kelvin. The fractional change in $\Lambda$ thus proposed and supported is

$$\left. \frac{\partial(ln\Lambda)}{\partial t} \right|_{\sigma} = -(\varphi S_w)^{1.33m}(1-\varphi)^{1.33n} A T e^{-E/(RT)} \tag{4}$$

or equivalently

$$\left. \frac{\partial(ln(1-\phi))}{\partial t} \right|_{\sigma} = +(\varphi S_w)^{1.33m}(1-\varphi)^{1.33n} A T e^{-E/(RT)}. \tag{5}$$

The Arrhenius frequency factor, a, equals AT. Here $m$ and $n$ are expected to be close to 1.0 and greater than 0.5, contact areas being less than fractal because of the finite size of atoms. m and n may be different because water-to-grain and grain-to-grain interfaces differ. Notably this mechanism is primarily a dimensional argument and lacks terms relating to the sizes, shapes, and composition of pores and grains. ( For a different approach see Yang 2000.) Fractional water saturation, $S_w$ might reduce compaction but is set to 1 and omitted hereafter.
Equation 5 indicates that if both sides are multiplied by the 'surface correction',
${\varphi_{av}}^{1.33m}(1-\varphi_{av})^{1.33n}/(\varphi^{1.33m}(1-\varphi)^{1.33n})$,

the right hand side (RHS) will be independent of porosity

$$\left. \frac{\partial(ln(1-\varphi)}{\partial t} \right|_{\sigma} (\varphi_{av}^{1.33m}(1-\varphi_{av})^{1.33n})/(\varphi^{1.33m}(1-\varphi)^{1.33n}) = A T e^{-E/(RT)} (\varphi_{av}^{1.33m}(1-\varphi_{av})^{1.33n}). \tag{6}$$

Factors like $\varphi_{av}$ and $T_{av}$ are averages over a 'well' which help visualization by minimizing movement of data on individual plots and among plots.

Further, if both sides of the equation are divided by the transition-state pre-exponential temperature, $T/T_{av}$, the 'temperature correction', the RHS and hence LHS will be independent of porosity and also of kinetic temperature, and in a form for estimating activation energy E,

$$\left.\frac{\partial(ln(1-\varphi)}{\partial t}\right|_{\sigma} (\varphi_{av}^{1.33m}(1-\varphi_{av})^{1.33n})/(\varphi^{1.33m}(1-\varphi)^{1.33n})(T_{av}/T) = AT_{av}e^{-E/RT}(\varphi_{av})^{1.33m}(1-\varphi_{av})^{1.33n}. \tag{7}$$

Again, Equation 7 means porosity itself must be constant in the LHS. This can be checked by transforming the experimental porosities in 'well' porosity-depth plots, as indicated, and shown here for six examples(Aoyagi and Asakawa, 1980, Fowler, Velda 1996, Athy 1930, Hedberg 1936). The examples are referred to here as 'wells' although they often combine porosities from several local wells. The Macran porosity data sets are inferred entirely from seismic data, not well data. The "Sulu Sea" data are a composite of several mostly unspecified wells.

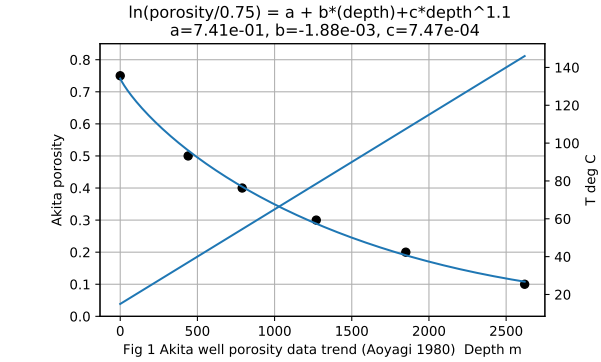


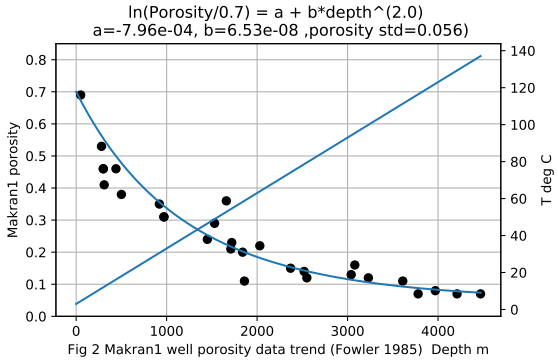


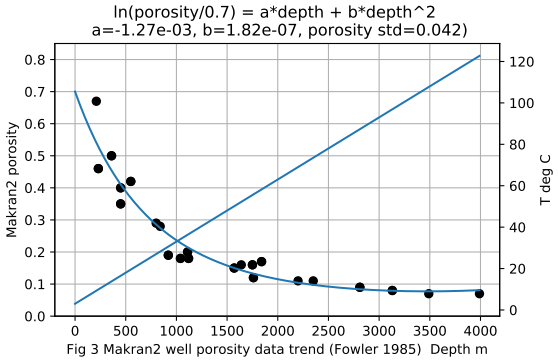


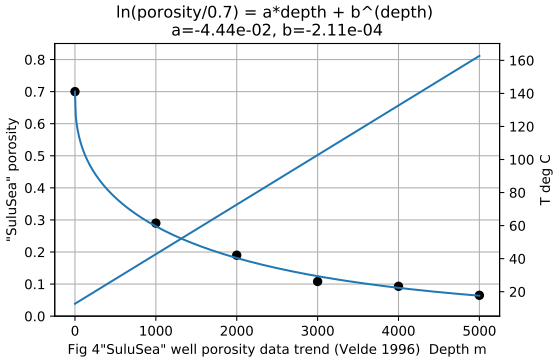


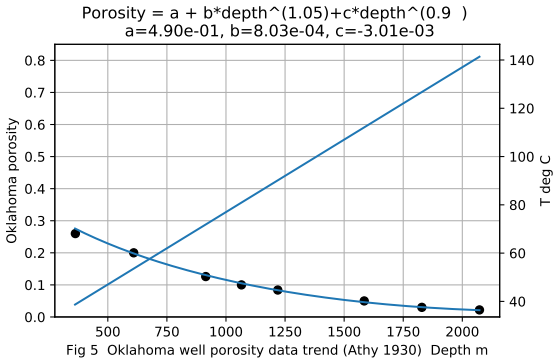


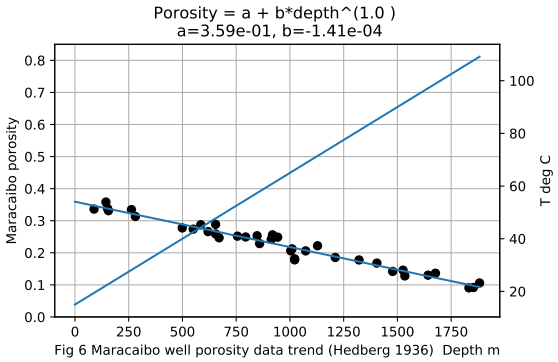


Figures 1-6 show the experimental example porosity-depth relations which were discussed recently ( Mondol, Bjrlykke,Jahren,and Heg 2007; Puttiwongrak,Giao,and Vann 2020). Curve fit equations are shown at the top of each plot. As seen in the figures the plotted maximum paleotemperature is always assumed to be a linear function of depth, separately for each 'well'.
It is perspicuous to view transformed porosities versus $\Lambda$ as a more fundamental variable than depth, common to all 'wells'. Figures 7-12 show

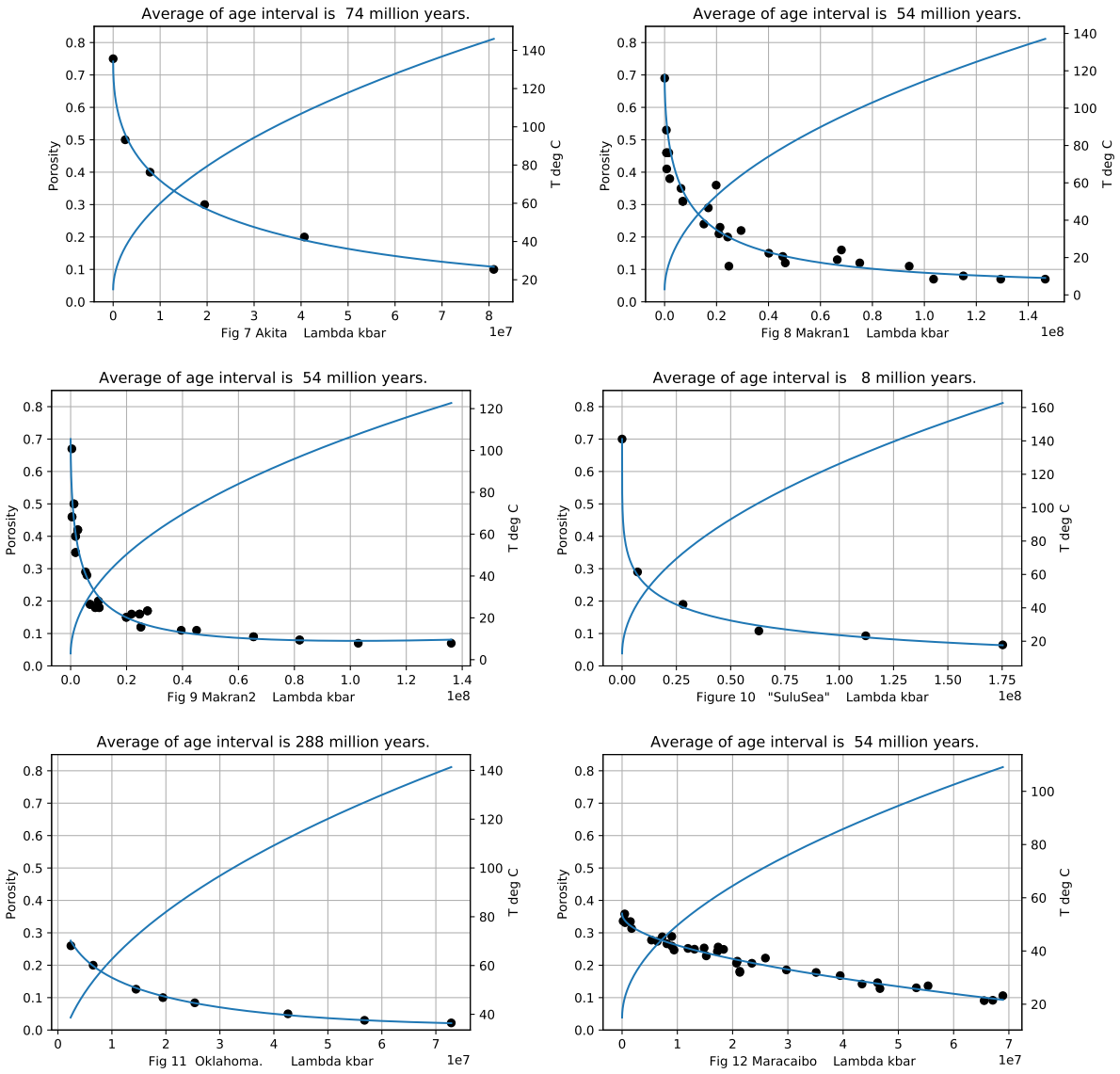


the porosity data versus an approximate $\Lambda$ horizontal axis. ( The approximation $p_w = g\rho_w z$ for normal water pressure is used to approximate the $\Lambda$ axis as

$$\Lambda \approx g\frac{(\rho_g - \rho_w)}{(1-\varphi)}\int_0^z (1-\varphi)dz. \tag{8}$$

Here $z$ is sample depth and depth 0 is the sediment-water or -air interface. The grain density and water density are $\rho_g$ and $\rho_w$. The water pressures in these wells were not given.) Any mismatch of experimental porosity with approximate $\Lambda$ is not important for illustrative purposes as porosity data points in non-normally-pressured zones are only shifted horizontally, e. g., overpresssured zones appear shifted to the right, and transformed porosity points are shown here to be nearly constant. Figures 13-18 show the porosities after the 'surface correction' Equation 5. The corrected porosities have largely moved toward a common value in each well.

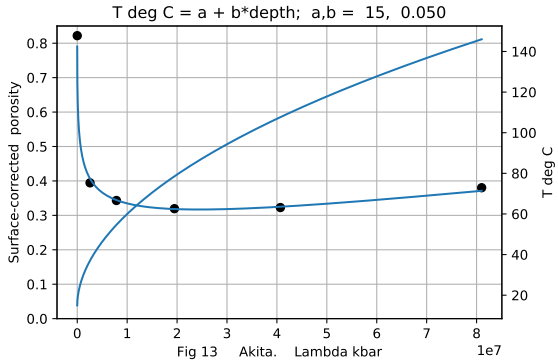


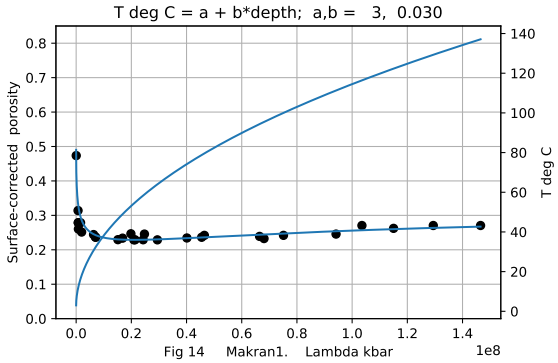


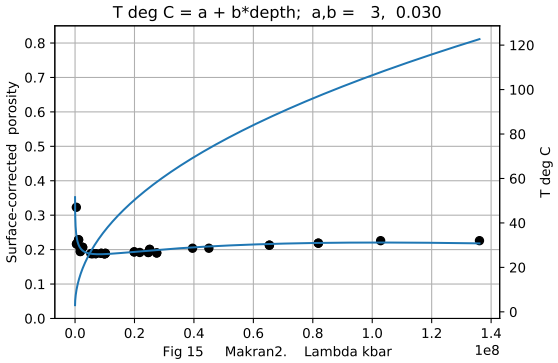


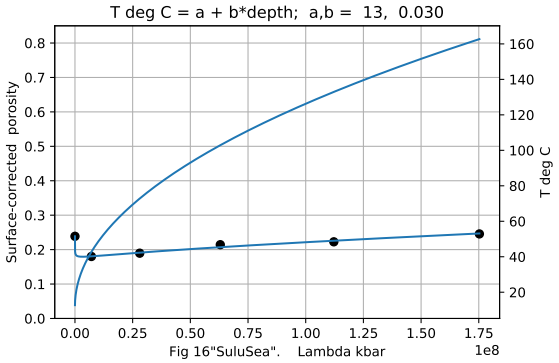


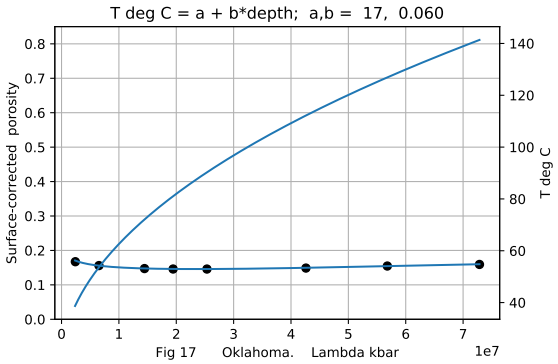


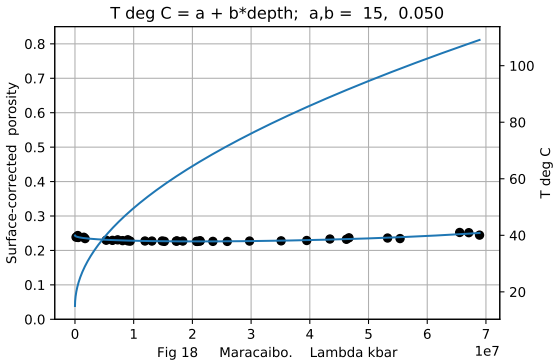


Figures 19-24 show the porosities after the second 'temperature correction', Equation 7.

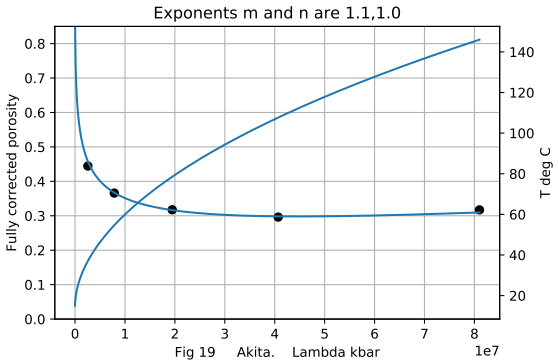


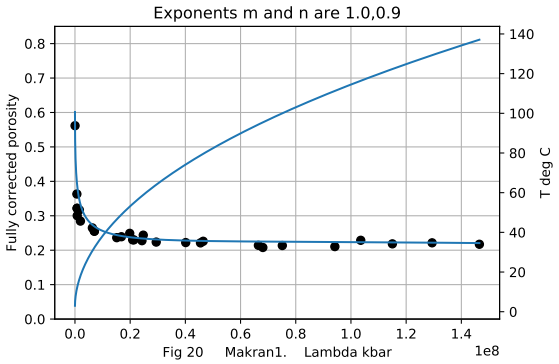

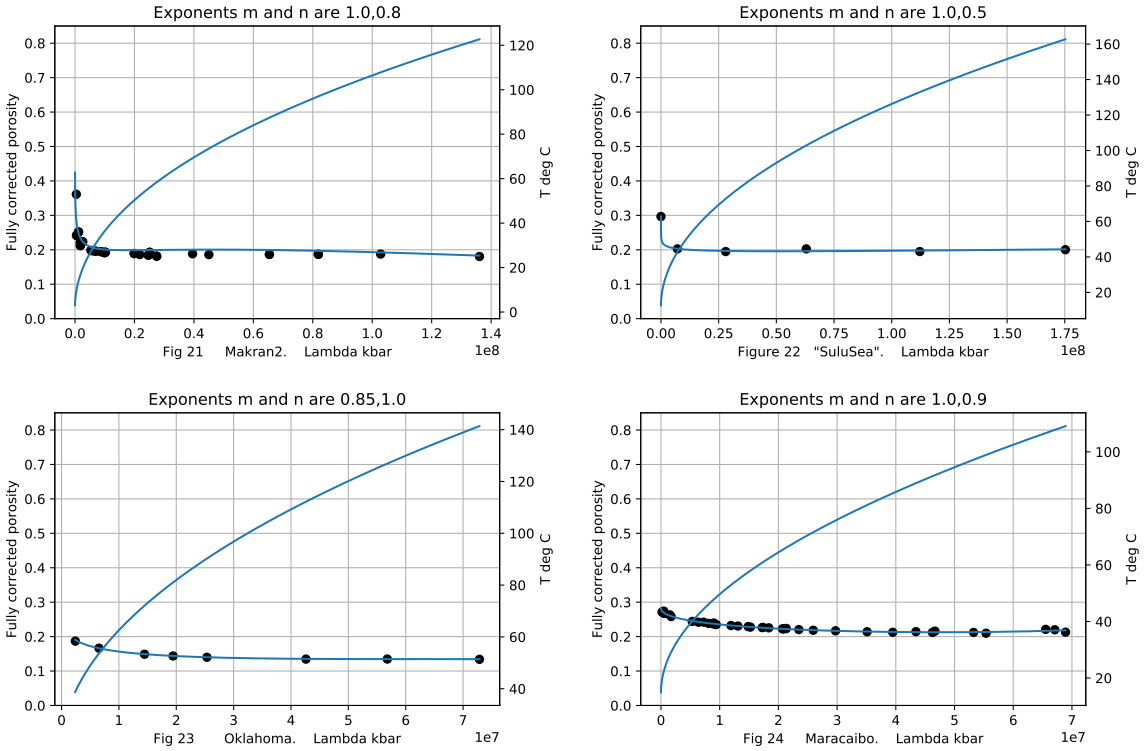


These figures immediately show that 1-the reaction is slow at temperatures below 30-40 C, 2-longer geologic times (Table 1) produce greater compaction effects and, 3-looking back to Figures 1-18 the 'temperature correction' is much smaller than the 'surface correction'. This means crucially that only approximate estimates of maximum paleo sediment-surface temperatures and geothermal gradients are needed.

# 7 Results

After both corrections, porosities in each well have approached a common value except for shallow low-temperature portions, supporting Equation 4. Table 1 gives the ratio of the entropy of the porosities after the corrections to the entropy before the corrections. The convergence of the transformed porosities is very good above 30-40 C.
An estimate of activation energy, E, can be made by plotting the logarithm of the left hand side of Equation 6 versus $-1/RT$. Cancelling out the common $\varphi_{av}$ terms Equation 6 becomes

$$\varphi^{-1.33m}(1-\varphi)^{-1.33n}(T_{av}/T)\left.\frac{\partial(ln(1-\varphi)}{\partial t}\right|_{\sigma} = Ae^{-E/RT}. \tag{9}$$

Breaking geologic time $\tau$ into many, N, small time increments $\delta t$ it is seen that each term in the sum below is the instantaneous time derivative $ln((1-\varphi_i)/(1-\varphi_{i-1}/\delta t$ for that time. The sum is the average over time of these instantaneous time derivatives and, like the pages of a book, add up to give the (large) finite-difference approximation on the right below, equivalent to only the starting and ending pages of the book as it were.

$$\Sigma_1^N(ln[(1-\varphi_i)/(1-\varphi_{i-1})])/N\delta t = ln[(1-\varphi)/(1-\varphi_0)]/|\tau| \tag{10}$$

Here we have put $\varphi_N = \varphi$, the current porosity. Porosity changes due to lateral forces and vertical forces are obviously included in the summation of the average, which is used in place of the partial derivative,

$$\left.\frac{\partial(ln(1-\varphi)}{\partial t}\right|_{\sigma} \rightarrow ln[(1-\varphi)/(1-\varphi_0)]/|\tau|. \tag{11}$$

This partial derivative on the left of Equation 11 would have come up in the same way if $\sigma$, Equation 3, represented horizontal forces rather than vertical forces. This approximation, or replacement, thus represents overall porosity reduction due to the combined forces and temperatures acting, in natural order, and including changes in overburden and pore fluid pressure, to reduce $\Lambda$. This replacement is more appropriate than the partial derivative for computing activation energy, and further cannot be avoided since the actual porosity data result from all these factors. Putting this approximation into Equation 9 gives

$$\varphi^{-1.33m}(1-\varphi)^{-1.33n}(T_{av}/T)ln((1-\varphi)/(1-\varphi_0))/\tau = Ae^{-E/RT} \tag{12}$$

Multiplying the LHS with a constant K to compensate for a possible mis-estimate would not change the estimate of E, as taking the slope of the logarithm of Equation 12 drops out both $\tau$ and K. Thus

$$E = -\Delta(ln(LHS^*)/\Delta(1/RT^*), \tag{13}$$

where the * superscript means at temperatures above $\approx$ 40C.

$$A = (LHS^*)\exp(E/RT^*). \tag{14}$$

With this E a rough approximate A is obtained evaluated at $\varphi^*_{av}$ and $T^*_{av}$, Table 1,

$$A = (LHS^*_{av})\exp(E/RT^*_{av}). \tag{15}$$

This A estimate would contain poorly known $\tau$ and any K. K = 1 is used. For $\varphi_0$, the largest surface porosity encountered in a well is used since the RHS and hence the LHS can not change sign. The average of the top and bottom geologic time boundaries for a 'well' is taken for $\tau$ in computing A. Plotting the log of the LHS versus $-1/RT$ gives E for the six 'wells', Figures 25-30.

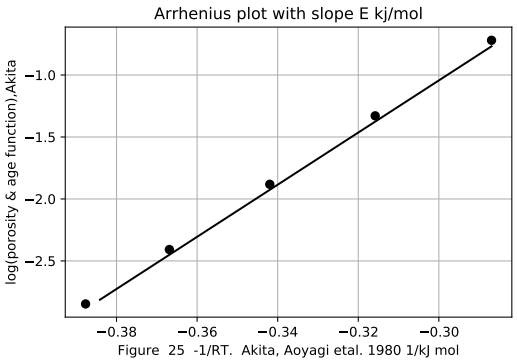

Figure 25 -1/RT. Akita, Aoyagi etal. 1980 1/kJ mol

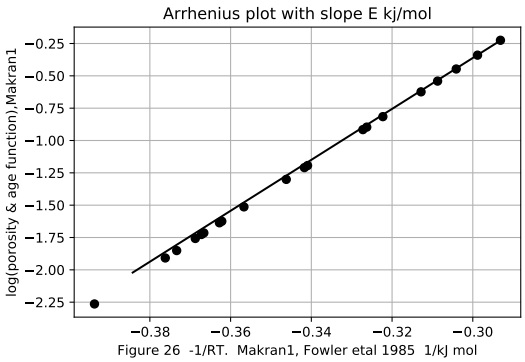

Figure 26 -1/RT. Makran1, Fowler etal 1985 1/kJ mol

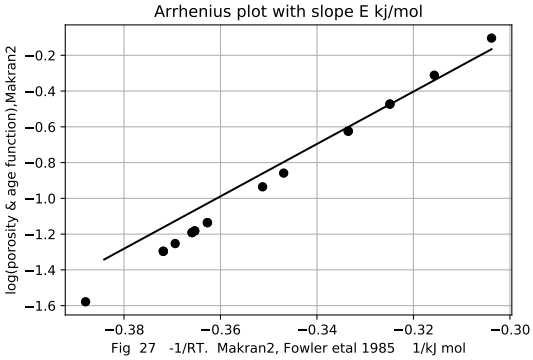

Fig 27 -1/RT. Makran2, Fowler etal 1985 1/kJ mol

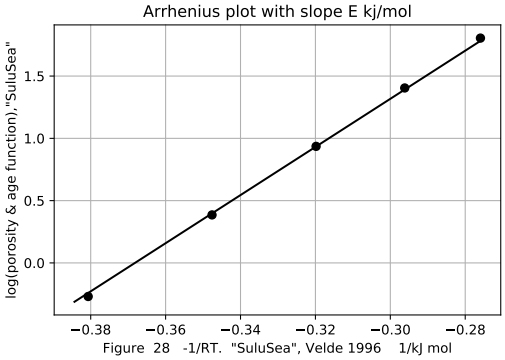

Figure 28 -1/RT. "SuluSea", Velde 1996 1/kJ mol

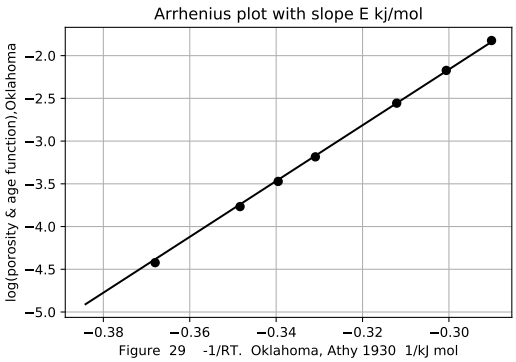

Figure 29 -1/RT. Oklahoma, Athy 1930 1/kJ mol

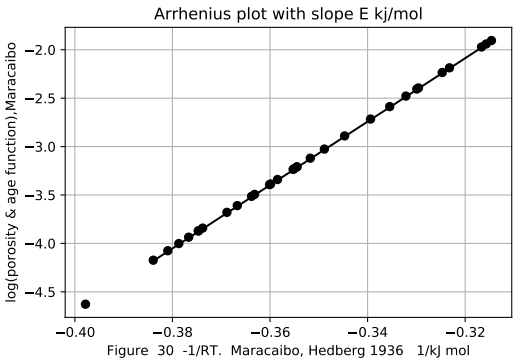

Figure 30 -1/RT. Maracaibo, Hedberg 1936 1/kJ mol

As shown in Table 1 the E's vary from 18 to 33 kJ/mol, averaging 24+-7 kJ/mol. Laboratory measurements of the pressure solution of quartz aggregates ( Miyakawa and Kawabe I 2014) also give 24 kJ/mol, and it is tentatively assumed that this is the rate-limiting reaction occurring in shales.

# 8 Discussion and Data

Map coordinates were known only for the Makran 'wells'. Temperatures were not available for any wells. Paleo mudline temperature estimates are made on the basis of paleoenvironments(Aoyagi K and Asakawa T 1980), paleolatitude, and geologic age, Table 2. Mudline temperatures of 3 C are assigned to wells from abyssal plains. Shallow sea or lake environments are assigned expected land paleotemperatures, corrected for paleolatitudes, and for any intervening high temperature events such as the Eocene high (Janke 2013). If two estimates are made they are averaged. The mudline temperature used for the Sulu Sea, 13 C, was measured at the deepest point (Lukens 1931).
These paleo-mudline-temperature estimates are less important to this study than are paleo-geothermal-gradients, as the compaction reaction found here becomes noticable at the higher 'well' temperatures. Because the Earth is cooling as radioactivity and initial energy of assembly decline, and because these wells were drilled/investigated in areas where temperatures were supposed to be high enough to generate petroleum, minimum paleo-geothermal-gradients of .03 C/m were initially assigned. The 'well' mudline and temperature gradient estimates used here are well within present day experience ( Christie and Nagihara, 2016).
A paleo-geothermal-gradient of .05 C/m was assigned to the Akita 'well', and to Maracaibo back-arc well, on the basis of necessary thermal maturity (Aoyagi K and Asakawa T 1980).
In Northeast Oklahoma nearby sedimentary rock mineralization and granite outcrop suggest a higher paleo-geothermal-gradient, perhaps .06 C/m as assigned, Table 1. Averaging the E's computed from all these provisional temperature gradient assignments, along with the one laboratory measurement, gives an average activation energy of 23+-6 kJ/mol. With this $E_{av}$ an Oklanoma paleo-geothermal-gradient of 0.12 C/m was computed. Also using this $E_{av}$, better paleo-geothermal-gradients for the other wells were obtained. These improved estimates with other recalculated parameters are shown in Table 3.
Reverting to discussing the process of estimating m and n, the uncertainties in paleotemperatures initially limited accuracy of activation energy estimates, but the 'temperature correction' contribution is small compared to the 'porosity correction' so does not detract much from the experimental validation of Eq 4. Current temperature profiles are known privately for thousands of wells. This information would help gain an accurate $E_{av}$, especially for deep-water wells where the paleo-mudline temperature is probably $\sim$ 3 C. Laboratory data for pressure solution of quartz and other minerals can be expanded to higher temperatures and pressures to check current ideas.
The Makran data, Figures 2 and 3, show that lateral forces in the accretionary wedge (Makron2) produced porosities reduced from nearby abyssal plain (Makron1) porosities. There the major lithology need not be clay throughout, as good reflectors were needed to produce data. The low Oklahoma porosities were also thought to have been reduced by lateral forces (Athy 1930; Hedberg 1936). Directionally variant lateral forces are often observed in horizontal drilling (Bjornen K 2019, private

communication). The compaction response mechanism to both vertical and horizontal forces is probably the same, Equation 4.

# 9 Conclusions

Equation 4 explains shale compaction at temperatures above $\approx$ 35 C with activation energies E $\approx$ 24+-6 kJ/mol, probably corresponding to pressure solution of quartz. Problems of mineralogy, grain shapes and sizes, permeability, overpressures and pore connectivity are by-passed. The results support nearly fractal pore interfaces with m $\approx$ 1. The matrix index ,n, is smaller for Sulu Sea and Macron2 'wells' suggesting smoother matrix for the geologically younger Sulu Sea 'well', although this pushes the data. The reduction in $\Lambda$ is also proportional to geologic age to the first power. By Equation 12 the one-dimensional problem is recognized as three spacial dimensions. Subsequently the geologic age effectively drops out while obtaining activation energy, and provisional paleotemperature gradients are used to bootstrap to better paleotemperature gradients. Given porosity-depth data and average activation energy, $E_{av}$, one can infer or rank maximum paleo-geothermal-gradients and from that organic maturity, thus avoiding unnecessary drilling.

Table 1 Derived variables for initially assumed paleotemperatures

| Basin Location | Basin type | Age range my | E kJ/mol | A $10^{12}$/sec | Entropy, relative | m | n |
|---|---|---|---|---|---|---|---|
| Akita, | back-arc | 1.5-146 | 21 | 3 | 0.7 | 1.1 | 1.0 |
| Hokkaido | | | | | | | |
| Makran1 | abyssal | 2.6-105 | 20 | 6 | 0.5 | 1.0 | 0.9 |
| Makran2 | abyssal | 2.6-105 | 18 | 8 | 0.4 | 1.0 | 0.8 |
| Sulu Sea | deep-water | 0-15 | 20 | 45 | 0.2 | 1.0 | 0.5 |
| Oklahoma | convergent | 254-323 | 33 | 1 | 0.2 | 0.85 | 1.0 |
| Maracaibo | back-arc | 2.58-105 | 33 | 1 | 0.3 | 1.0 | 0.9 |

Table 2 Description and initial parameters for wells

| Basin Location | Basin type | Age range my | Paleo- mudline C | Paleo $\nabla T$ C/m | References |
|---|---|---|---|---|---|
| Akita, | back-arc | 1.5-146 | (3+13+13)/2 | .05 | Aoyagi et al. |
| Hokkaido | | | | | pp 41 |
| Makran1 | abyssal | 2.6-105 | 3 | .03 | Fowler et al. |
| Makran2 | abyssal | 2.6-105 | 3 | .03 | pp 429-430 |
| Sulu Sea | deep-water | 0-15 | 13 | .03 | Velde pp 196 |
| Oklahoma | convergent | 254-323 | (7+14+13)/2 | .06 | Athy pp 12 |
| Maracaibo | back-arc | 2.58-105 | (3+14+13)/2 | .05 | Hedberg pp 254 |

Table 3 Inferred parameters for $E_{av}$ = 24+-6 kJ/mol

| Basin Location | Age range my | Paleo $\nabla T$ C/m | E kJ/mol | A $10^{12}$/sec | Entropy, relative | m | n |
|---|---|---|---|---|---|---|---|
| Akita, Hokkaido | 1.5-146 | 0.04 | 24 | 3 | 0.7 | 1.1 | 1.0 |
| Makran1 | 2.6-105 | 0.02 | 22 | 8 | 0.5 | 1.0 | 0.9 |
| Makran2 | 2.6-105 | 0.02 | 24 | 11 | 0.3 | 1.0 | 0.8 |
| Sulu Sea | 0-15 | 0.02 | 25 | 43 | 0.2 | 1.0 | 0.5 |
| Oklahoma | 254-323 | 0.12 | 24 | 0.9 | 0.5 | .85 | 1. |
| Maracaibo | 2.58-105 | 0.09 | 24 | 0.9 | 0.6 | 1.0 | 0.9 |

Author contributions: All work done by corresponding author James Eward Smith 85, with physicist son Edward Millard Smith-Rowland as backup due to age and Covid 19 threat.
Funding: This research received no external funding.
Conflicts of interest: The authors declare no conflict of interest.

## 10 References

Aoyagi K, Asakawa T(1980) Primary migration theory of petroleum and its applicationn to petroleum exploration. Organic Geochem 2 pp 33 - 43

Athy, LF,(1930) Density, porosity, and compaction of sedimentary rocks. Amer Assoc of Petroleum Geol Bull 14 1 pp 1 - 24

Christie, CH and Nagihara, S(2016) Geothermal gradients of the northern continental shelf of the Gulf of Mexico. Geosphere 12 1 pp 26 - 34

Fowler, SR, White, RS, Louden, KE,(1985) Sediment dewatering in the Makran accretionary prism. Earth and Planetary Science Letters 75 4, pp 427 - 438

Hedberg, HD,(1936) Gravitational compaction of clays and shales. Amer J of Science 31 184 pp 241 - 287

Janke,PR (2013) A correlated history of Earth. Pan Terra Inc. The worldwide museum of natural history.

Lukens RR(1931) Surveying the Phillipine Islands. NOAA History; Merchant Marine Bull Apr 1931 pp 10,11,32

Miyakawa K, Kawabe I(2014) Pressure solution of quartz aggregates under low effective stress (0.420.61 MPa) at 2545 C. Applied Geochem 40 pp 61 - 69

Mondol NH ,Bjrlykke K, Jahren J, Heg K(2007) Experimental mechanical compaction of clay mineral aggregates. Changes in physical properties of mudstones during burial. Marine and Petroleum Geol 24 5 pp 289 - 311

Puttiwongrak A, Giao PH, Vann S(2020) An easily used mathematical model of porosity change with depth and geologic time in deep shale compaction. Inter J of GEOMATE 19 73 pp 108-115

Smith JE(1971) The dynamics of shale compaction and evolution of pore-fluid pressures. J Inter Assoc for Mathematical Geology 3 3 pp 239 - 263

Smith JE, Dysinger GC, Borst RL(1980) Shales and abnormal pressures. In:Saxena, S K(ed)Geotechnical and Environmental Aspects of Geopressure Energy. Engineering Foundation,New York, pp 69-91

Velde, B(1996) Compaction trends of clay-rich deep sea sediments. Marine Geology 133 3-4, pp 193 - 201

Yang X(2000) Pressure solution in sedimentary basins: effect of temperature gradient.Earth and Planetary Science Letters Volume 176, Issue 2, 15 March 2000, pp 233 - 243